Initial growth stages of titanium and barium oxide films on SrTiO$_3$(001)

Chen Wu, Karen Kruska, Martin R. Castell *

Department of Materials, University of Oxford, Parks Road, Oxford OX1 3PH, UK

ARTICLE INFO

ABSTRACT

Ultrathin titanium and barium oxide films were grown on SrTiO$_3$(001) substrate surfaces via Ti/Ba deposition and oxidation. When Ti is deposited onto the SrTiO$_3$(001) surface, it forms a series of SrTiO$_3$ surface reconstructions such as c(4 × 2), $\left(\sqrt{5} \times \sqrt{5}\right)-R26.6°$, (6 × 2) and (9 × 2), which can be controlled by varying the Ti concentration. Epitaxial anatase TiO$_2$(001) islands with (1 × 3) and (1 × 5) reconstructions are formed by further increasing the Ti deposition amount and post-annealing. The initial growth of BaO thin films depends on the surface condition of the substrate. BaO nanoparticles form on reconstructed SrTiO$_3$(001), while a locally ordered c(4 × 4) BaO structure is observed on the disordered sample surface. Co-deposition of Ba and Ti on SrTiO$_3$(001) results in phase separation with the deposited Ba forming BaO nanoparticles and the Ti contributing to Ti-rich SrTiO$_3$ surface reconstructions. No formation of BaTiO$_3$ is observed at the initial growth stages between 0.3 monolayer (ML) and 1.8 MLs.

1. Introduction

Interest in the growth of titanium and barium oxide thin films has been stimulated by a variety of potential applications. For example, TiO$_2$ thin films have been used in catalysis [1–3], gas sensing [4–6] and solar energy conversion [7–9], while BaO finds applications including high current density cathodes [10–12], thermionic energy converters [13] and optical devices [14–16]. The properties utilized in these applications are partially determined by the film structure, in which the substrate for the thin film growth plays an essential role.

SrTiO$_3$(001) surfaces serve as suitable substrates for the thin film growth of anatase TiO$_2$, BaO, and BaTiO$_3$ if both oxides are grown simultaneously or as alternative layers. This is because of a small lattice mismatch between the film and the substrate (3.1% for anatase TiO$_2$ and SrTiO$_3$, 0.3% with a 45° rotation of the BaO(001) surface with respect to the SrTiO$_3$(001) surface, and 2.3% for BaTiO$_3$ and SrTiO$_3$). Despite extensive interest in TiO$_2$ [17–20], BaO [21–23] and BaTiO$_3$ [24–26] thin film growth on SrTiO$_3$(001) surfaces, very few studies have been performed on the detailed initial growth stages of these films on the SrTiO$_3$ substrate. Especially, surface reconstructions have recently been reported to play an important role in the growth of perovskite oxides on SrTiO$_3$(001) surfaces with epitaxial growth achieved on the (2 × 1)-reconstructed substrate but not on the c(6 × 2) reconstruction [27]. It is therefore important to study film growth that takes SrTiO$_3$ substrate structures into consideration, since the substrate surface reconstruction may have significant influence on the initial growth steps and hence the overall film quality.

In this paper, we report a study where both reconstructed and disordered SrTiO$_3$(001) substrate surfaces are used for the early growth stages of TiO$_2$ and BaO thin films. The possibility of the formation of BaTiO$_3$ by either Ba deposition on a Ti-rich SrTiO$_3$(001) surface or Ba & Ti deposition is also explored. The surface structures are characterized using low energy electron diffraction (LEED) and scanning tunneling microscopy (STM) following each deposition step. For the initial growth of TiO$_2$ on SrTiO$_3$(001), the deposited Ti forms a series of Ti-rich SrTiO$_3$(001) reconstructions. Increased Ti coverage and/or post-annealing lead to the formation of epitaxial anatase islands. The growth mode of BaO on SrTiO$_3$(001) surfaces is significantly affected by the substrate surface. Reconstructed SrTiO$_3$(001) surfaces result in the formation of BaO nanoparticles whereas c(4 × 4) reconstructed BaO terraces are observed using a disordered SrTiO$_3$(001) substrate surface. No indication of BaTiO$_3$ is seen when both Ba and Ti are deposited on the substrate at the initial growth stage. Instead, Ba forms BaO nanoparticles on the surface while Ti contributes to Ti-rich SrTiO$_3$(001) reconstructions such as the c(4 × 2) reconstruction and surfaces decorated with ordered nanostructures.

2. Experimental details

The experiments were carried out in a JEOL JSTM4500XT ultrahigh vacuum (UHV) system, operating at a base pressure of 10^{-8} Pa. Epi-polished (001) surfaces of SrTiO$_3$ single crystals (PI-KEM Ltd., UK) were used as substrates for the thin film growth. To achieve electrical conductivity and therefore suitability for STM imaging and LEED investigation, the samples were 0.5 wt.% Nb-doped. SrTiO$_3$ samples were sputtered and/or annealed in UHV to form suitable substrate surfaces prior to metal deposition. Ti was deposited from an electron beam

* Corresponding author.
E-mail address: martin.castell@materials.ox.ac.uk (M.R. Castell).

evaporator (Oxford Applied Research EGN4) using 99.99% pure Ti rods (Johnson Matthey plc, UK), while Ba deposition was performed using a getter wire (SAES Getters S.p.A.) installed in a dedicated Ba evaporator built in the Institute of Physics and Physical Technologies at the Technical University of Clausthal. The films were oxidized with three oxygen sources: residual gases in the chamber, the substrate, and purposeful admission of gaseous oxygen. As the Ba and Ti sources are located in separated chambers, they could not be deposited at the same time. However, we refer to the process as 'co-deposition' if Ti is deposited onto the sample surface immediately after Ba deposition prior to oxidation. All STM images were taken from room temperature (RT) samples, and the surface coverage was estimated by comparing the Ti/Ba deposition amount on clean Au(111) surfaces under the same deposition conditions.

3. Results

3.1. Early growth stages of epitaxial anatase TiO$_2$ films on SrTiO$_3$(001)

3.1.1. Surface structure evolution with increasing Ti coverage

Ti was deposited onto the SrTiO$_3$(001) surface and oxidized by residual gases in the chamber and/or oxygen from the substrate. The STM images in Fig. 1 show the evolution of surface structures with increased Ti deposition. The substrate surface shown in Fig. 1a was obtained by UHV annealing the SrTiO$_3$(001) sample at 1050 °C for 30 min. The surface contains small ordered regions with bright spots

ordered along the [110] and $[1\bar{1}0]$ directions. The measured periodicity (11.2 ± 0.4 Å) indicates a c(4 × 4) reconstruction. Decreasing the imaging bias results in the observation of another structure, a (2 × 2) reconstruction shown in Fig. 1 in the Supporting information (SI). This is consistent with a previous study that the c(4 × 4)-SrTiO$_3$(001) reconstruction forms an adlayer on the (2 × 2) and both structures can be probed on the same surface region when different sample biases are applied [28].

Fig. 1b shows an STM image taken after depositing 0.10 ML of Ti onto the reconstructed SrTiO$_3$(001) surface at 450 °C. The substrate temperature was held at 450 °C for 30 min before and after the deposition procedure, allowing the formation of equilibrium structures. Small islands with a round shape start to form on the substrate surface following the deposition. The islands are measured to be approx. 4 Å in height and appear distributed evenly over the substrate surface with no preference for nucleation at the step edges. The c(4 × 4) reconstruction of the SrTiO$_3$(001) substrate is still visible in the background. An increased Ti deposition amount of 0.25 ML on a clean sample surface leads to the formation of larger islands with straight edges aligned with the crystal directions of the substrate (Fig. 1c). The measured height of the islands remains approx. 4 Å.

An STM image of a sample surface following 0.50 ML of Ti deposition is shown in Fig. 1d. It appears that the rectangular islands in Fig. 1c become larger to form a maze structure with step edges aligned with the [010] and [100] crystallographic directions of the substrate. The step height (approx. 4 Å) remains unchanged. A row structure is seen on
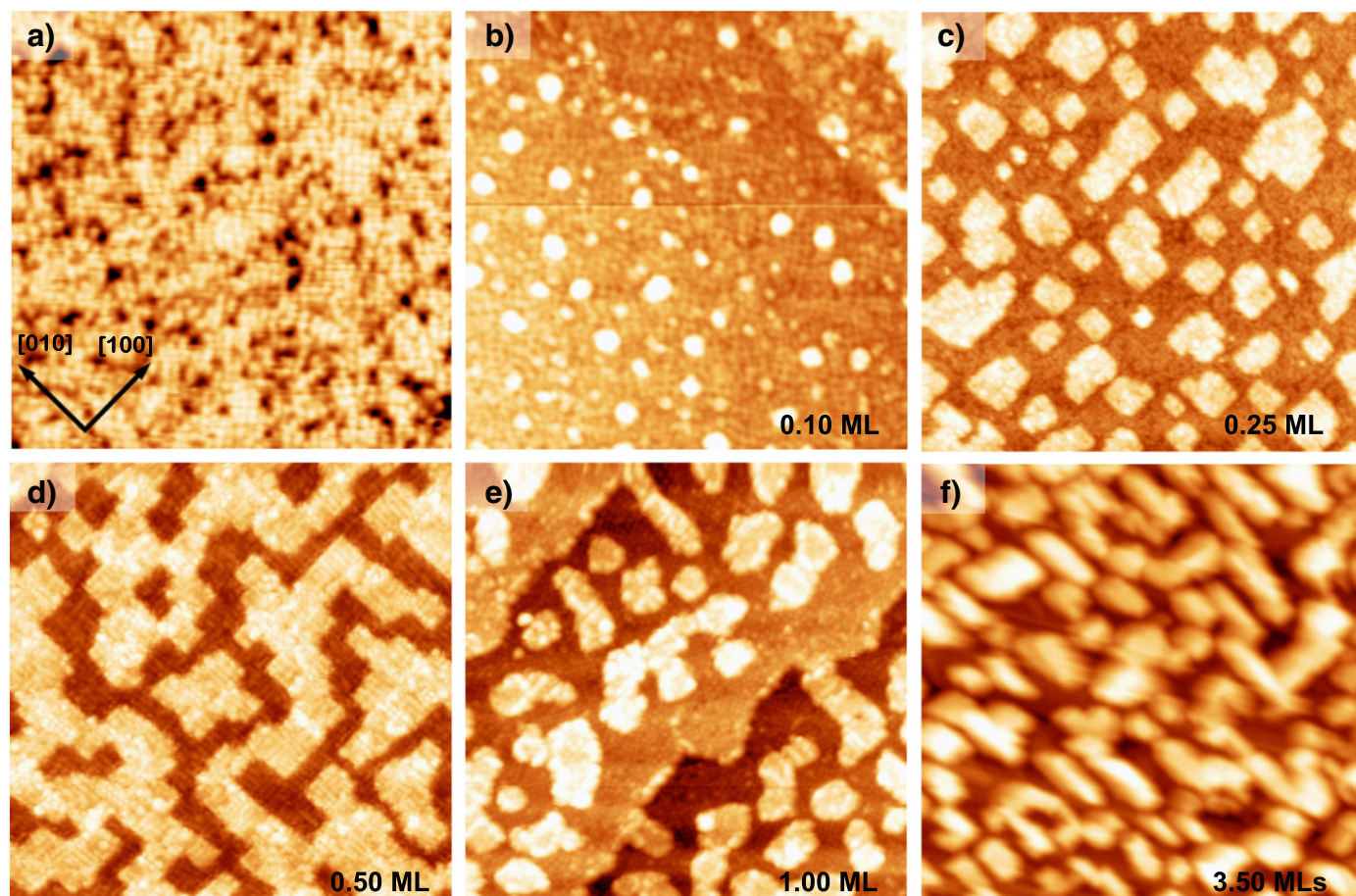
Fig. 1. Increasing amounts of Ti were deposited onto the reconstructed SrTiO$_3$(001) surface held at 450 °C. The temperature was maintained prior to and after Ti deposition to allow the formation of equilibrium structures. (a) c(4 × 4) reconstructed SrTiO$_3$(001) substrate surface with patches of ordered bright spots (Image size: 50 × 50 nm^2, V$_s$ = 2.11 V, I$_t$ = 0.20 nA). (b) 0.10 ML: formation of small islands on the reconstructed SrTiO$_3$(001) surface (Image size: 60 × 60 nm^2, V$_s$ = 0.74 V, I$_t$ = 0.05 nA). (c) 0.25 ML: larger rectangular islands with the edges aligned with the [010] and [100] crystallographic directions of SrTiO$_3$(001) (Image size: 70 × 70 nm^2, V$_s$ = 1.28 V, I$_t$ = 0.19 nA). (d) 0.50 ML: a maze structure with a c(4 × 2) SrTiO$_3$(001) periodicity (Image size: 50 × 50 nm^2, V$_s$ = 0.86 V, I$_t$ = 0.30 nA). (e) 1.00 ML: areas of the $\sqrt{5} \times \sqrt{5} - R26.6°$ SrTiO$_3$(001) reconstruction (Image size: 70 × 70 nm^2, V$_s$ = 1.22 V, I$_t$ = 0.20 nA). (f) 3.50 MLs: bright anatase islands on the SrTiO$_3$(001) substrate (Image size: 100 × 100 nm^2, V$_s$ = 1.31 V, I$_t$ = 0.10 nA).

the islands in Fig. 1d, while a rhombus-shaped structure is observed under the same imaging conditions (SI, Fig. 2). This is probably due to whether a metal atom or oxygen atom is at the tip apex as previously observed on the c(4 × 2)-reconstructed SrTiO3(001) surface [29]. Given the large coverage of ordered structures, the surface can also be examined using LEED, which confirms the c(4 × 2) reconstruction (SI, Fig. 3). The reconstruction has previously only been observed on sputtered and annealed SrTiO3 samples, and its formation requires post-annealing in UHV at relatively high temperatures (around 900 °C) [30–32]. The results obtained here demonstrate that the same structure can be produced by a completely different route with a much lower annealing temperature (450 °C).

Further increasing the Ti coverage to 1.00 ML leads to a surface structure with irregular islands on the terraces as shown in Fig. 1e. The step edges are wavy and do not align with the substrate crystallographic directions. The surface is locally ordered and contains two domains, exhibiting an angle of approx. 36° with each other and an angle of approx. 27° with respect to the main crystal directions of the substrate. The periodicity is measured as approx. 8.9 ± 0.2 Å, indicating a $\left(\sqrt{5} \times \sqrt{5}\right)-R26.6°$ reconstruction, which is also confirmed by LEED (SI, Fig. 4).

The $\left(\sqrt{5} \times \sqrt{5}\right)-R26.6°$ reconstruction has previously been reported on SrTiO3(001) surfaces following UHV annealing at high temperatures (above 1000 °C) [33–37]. Two models have been proposed for the structure, a Sr adatom model [35–37] and an O vacancy model [33,34]. Observation of the Ti and O atoms in the $\left(\sqrt{5} \times \sqrt{5}\right)-R26.6°$ unit cell using high resolution STM has been reported recently, which challenges the Sr adatom model [38]. Our study also indicates that the $\left(\sqrt{5} \times \sqrt{5}\right)-R26.6°$ reconstruction formed by Ti deposition is very unlikely to contain a Sr adlayer because of the increased amount of Ti deposited compared with other Ti-rich SrTiO3(001) reconstructions.

Fig. 1f shows the surface following 3.50 MLs Ti deposition. Similar to Fig. 1c, the image contains rectangular islands aligned with the [010] and [100] directions. The island heights, however are much larger than that of the islands in Fig. 1c (approx. 4 Å). They vary from approx. 9.7 Å to 38.4 Å, which correspond to one to four unit cell heights of anatase TiO2 (9.5 Å). Although the height measurement of STM images may be slightly affected by electronic effects, anatase has been found to grow on the SrTiO3(001) substrate in various previous reports [19,20,39] as a result of the small lattice mismatch.

3.1.2. Post-annealing effect

Post-annealing facilitates the formation of the anatase islands with relatively low Ti coverages. On a sample with 0.50 ML Ti deposition (similar to that shown in Fig. 1d), nanolines start to form surrounded by the SrTiO3(001)-c(4 × 2) reconstruction following UHV annealing at 500 °C for 30 min. Arrows 'A' and 'B' in Fig. 2a indicate a diline and a triline structure, respectively. A SrTiO3(001)-(6 × 2) reconstruction has been determined for the diline [30] and a (9 × 2) reconstruction for the triline [40]. Their chemical composition and atomic structures have also been investigated [32,41,42]. Again, these nanolines were previously only obtained on sputtered SrTiO3(001) surfaces and were thought to evolve from the c(4 × 2) reconstruction with elevated annealing temperatures (950–1150 °C) [40,43].

Further UHV annealing at 600 °C for 30 min produces bright square islands on the nanoline- and c(4 × 2)-covered surface (Fig. 2b). The structure of the bright islands could not be resolved but the island height is measured as either approx. 4.8 Å or 9.6 Å, corresponding to half or a single unit cell height of anatase TiO2. Consequently, the islands are the first sign of epitaxial anatase TiO2 similar to those observed on sputtered and annealed SrTiO3(001) surfaces [43].
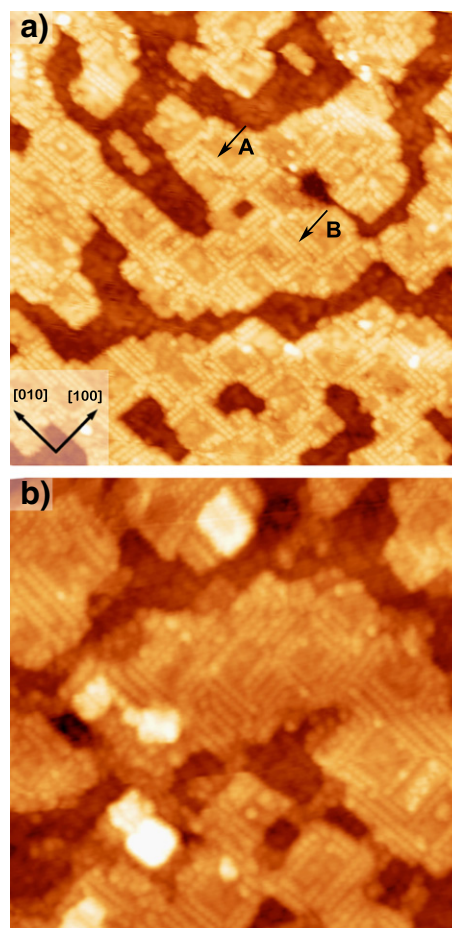
Fig. 2. (a) STM image of the diline and triline structures, indicated by arrows 'A' and 'B', on an annealed SrTiO3 surface with 0.50 ML of Ti deposition (Image size: 47 × 47 nm², V_s = 2.00 V, I_t = 0.20 nA). (b) STM image showing the appearance of bright square islands surrounded by nanoline structures on a sample surface with 0.50 ML Ti deposition and post-annealed at 600 °C for 30 min (Image size: 46 × 46 nm², V_s = 1.10 V, I_t = 0.28 nA).

Depositing 3.50 MLs of Ti and annealing at 600 °C for 30 min leads to a higher coverage of bright islands compared to the surface with 0.50 ML of Ti (Fig. 2b) and a surface fully covered with elongated nanolines (Fig. 3a). Further annealing at 600 °C for 4 h allows the observation of a row structure on the islands (Fig. 3b). The height of the islands (9.5 ± 0.3 Å) corresponds to the length of the long edge of the anatase TiO2 unit cell (9.5 Å), while it is measured as approx. 11.8 Å across the rows, approximately three times the short edge of the anatase unit cell (3.8 Å). The alignment of the island edges confirms the epitaxial relationship as TiO2(001) ||SrTiO3(001) and TiO2[010] ||SrTiO3[010] [20].

Fig. 4 shows LEED patterns taken from the surface with different electron beam energies. In Fig. 4a, multiple spots can be seen on the axes between the integer ones, indicating a two-domained (5 × 1) reconstruction. In the literature, several reconstructions on anatase TiO2(001) surfaces including (3 × 1), (4 × 1), (5 × 1) and (6 × 1) have been reported [43,44]. Based on combined STM and LEED data, it is likely that multiple reconstructions coexist on the anatase islands, among which the (3 × 1) structure is observed in the STM image shown in Fig. 3b. The (5 × 1) reconstruction, however, appears to be dominant on most of the surface and hence is detected by LEED. Fig. 4b shows a mixture of the (5 × 1) pattern contributed by the anatase islands and the c(4 × 2) reconstruction detected from the substrate layer.
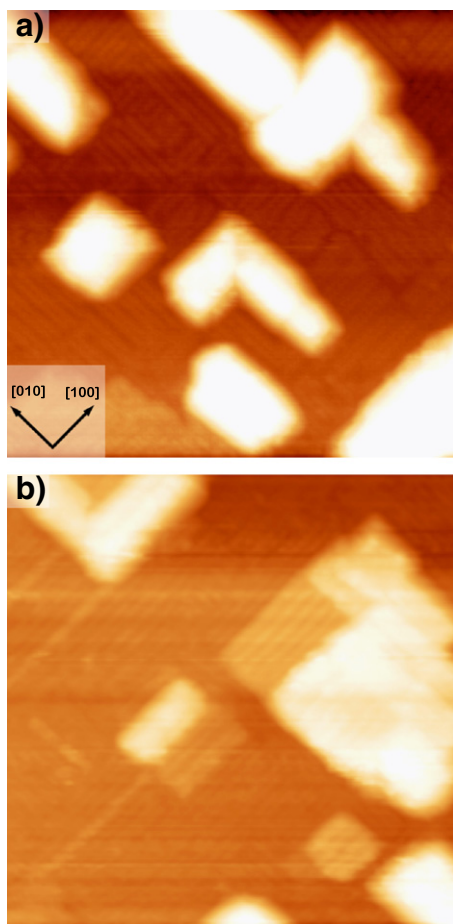
Fig. 3. (a) Depositing 3.50 MLs of Ti and post-annealing gives rise to a higher coverage of bright islands on the nanoline-covered SrTiO₃ surface. (Image size: 44×44 nm², $V_s = 0.85$ V, $I_t = 0.08$ nA). (b) Longer annealing time allows the observation of a row structure on the islands (Image size: 45×45 nm², $V_s = 0.83$ V, $I_t = 0.20$ nA).
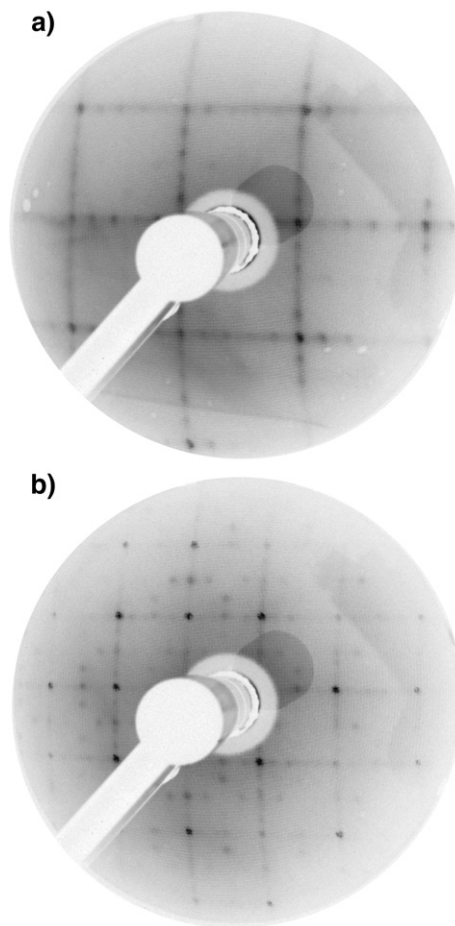
Fig. 4. LEED patterns of a sample surface with 3.50 MLs of Ti deposition, taken at electron beam energies of 63 eV and 147 eV, showing the (5×1) reconstruction in (a), and mixed (5×1) and $c(4 \times 2)$ reconstructions in (b).

3.2. Initial growth stages of BaO on SrTiO₃(001)

Ba deposition was performed using both reconstructed and disordered SrTiO₃(001) surfaces as the substrate. For the former, the SrTiO₃ sample was Ar⁺ sputtered with an ion energy of 0.5 keV and a flux of 86 µA/cm², and annealed in UHV at 870 °C for 30 min. This gives rise to a $c(4 \times 2)$-reconstructed SrTiO₃(001) surface similar to that shown in Fig. 1d. The surface has Ti-rich terraces with their edges aligned along the [010] and [100] directions of the substrate.

0.30 ML Ba deposition onto the substrate surface held at 300 °C gives rise to bright islands which may correspond to BaO nanoparticles on the $c(4 \times 2)$-reconstructed SrTiO₃(001) surface (Fig. 5a). On large-scale images, not shown here, the step edges of the surface appear wavy and are not strictly aligned with the main crystal directions. The step edges, however, can be straightened by post-annealing in UHV at 600 °C for 2 h (Fig. 5b). Re-appearance of the wavy steps is observed in Fig. 5c following an increased Ba amount of 0.90 ML on the same surface. Again, the straight step edges can be restored by UHV annealing at 600 °C for 2.5 h, as seen in Fig. 5d with more BaO nanoparticles on the substrate terraces. A larger number of BaO nanoparticles and terraces with irregular shapes are observed (Fig. 5e) with further increased Ba deposition (0.60 ML) onto the same surface held at RT followed by annealing in UHV at 450 °C for 45 min. The square terraces could not be recovered even with post-annealing at 600 °C for 2.5 h (Fig. 5f). The surface becomes unimagable when the Ba coverage is increased further. It is possible that with a significantly raised Ba amount, the insulating oxide film becomes too thick with an associated large resistance. Other SrTiO₃ reconstructions such as the (2×2) and $c(4 \times 4)$ have also been used as the substrate, which all lead to the formation of BaO nanoparticles.

A disordered substrate surface may provide more nucleation sites and a higher surface energy which may be beneficial for thin film wetting. A SrTiO₃(001) sample was sputtered to form a disordered surface as the substrate. Again, the growth temperature was kept at 300 °C for 30 min before and after Ba deposition (0.30 ML). In order to form smooth and ordered structures, the sample was then annealed in UHV at 850 °C for 1 h. Fig. 6a shows the annealed surface with small flat surface areas indicated by arrows. The structure forms steps mainly running along the [010] direction of the substrate. Fig. 6b shows an enlarged image taken from a flat region elsewhere on the surface. A unit cell is indicated on the image, rotated by 45° with respect to the step edges. The step height is measured as approx. 2.8 Å, corresponding to half unit cell height of BaO. Also, the measured periodicity (10.8 ± 0.5 Å) of the structure indicates a $c(4 \times 4)$ reconstruction on SrTiO₃(001). As the lattice mismatch between BaO and SrTiO₃ can be significantly reduced by a 45° rotation of the BaO lattice on SrTiO₃(001), it is likely that the rotated lattice corresponds to an epitaxial BaO structure.

3.3. Ba and Ti co-deposition on SrTiO₃(001)

The elemental growth of BaTiO₃ on SrTiO₃(001) may be achieved by two methods: growth of alternative TiO₂ and BaO layers and co-deposition of Ba and Ti followed by oxidation. In Section 3.2, Ti-rich
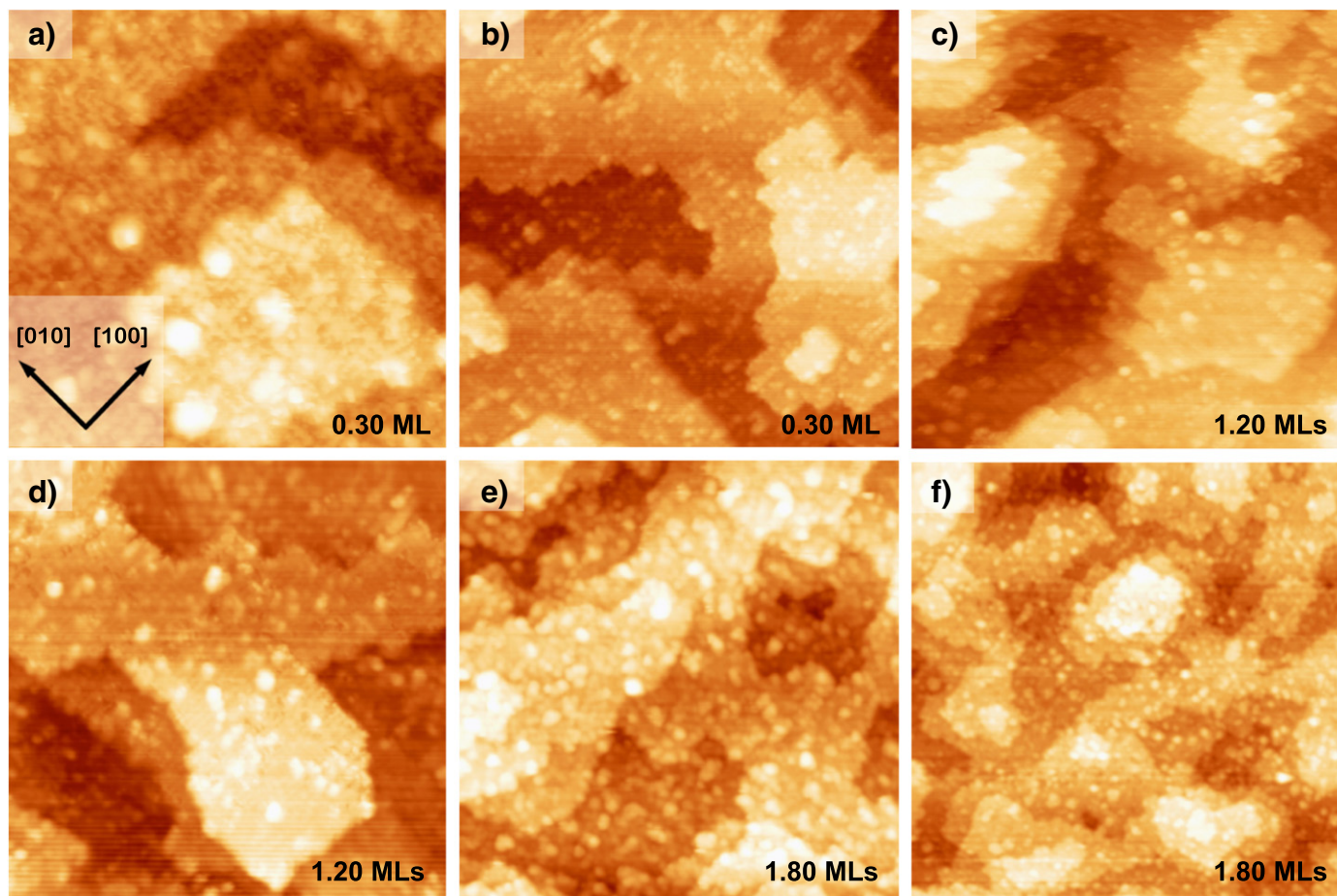
Fig. 5. STM images showing (a) BaO nanoparticles on the c(4 × 2)-reconstructed SrTiO₃(001) surface following Ba deposition and oxidation (Image size: 29 × 29 nm², $V_s = 0.69$ V, $I_t = 0.20$ nA); (b) straightened step edges as a result of post-annealing in UHV at 600 °C for 2 h (Image size: 59 × 59 nm², $V_s = 0.68$ V, $I_t = 0.20$ nA); (c) wavy step edges following further Ba deposition (Image size: 58 × 58 nm², $V_s = 0.55$ V, $I_t = 0.20$ nA); (d) increased coverage of BaO nanoparticles on the c(4 × 2) terraces with step edges straightened after UHV annealing at 600 °C for 2.5 h (Image size: 50 × 50 nm², $V_s = 0.88$ V, $I_t = 0.20$ nA); (e) BaO nanoparticles spread over the substrate surface (Image size: 70 × 70 nm², $V_s = 0.55$ V, $I_t = 0.20$ nA); (f) similar morphology as in (e) after post-annealing (Image size: 140 × 140 nm², $V_s = 1.23$ V, $I_t = 0.20$ nA).

SrTiO₃ substrates are used for Ba deposition. However, either BaO nanoparticles or epitaxial layers form instead of BaTiO₃. In order to further explore the possibility of BaTiO₃ formation via elemental growth at the initial stages, both Ba and Ti were deposited onto a clean unreconstructed SrTiO₃ surface. The sample was degassed at around 400 °C and cooled down to RT to avoid the formation of any Ti-rich reconstruction. Ba (0.50 ML) and Ti (0.50 ML) were then deposited onto the RT sample, followed by annealing in 10^{-6} Pa O₂ at 400 °C for 40 min. This leads to a disordered surface shown in Fig. 7a.

Annealing the sample in UHV at 800 °C for 1.5 h gives rise to bright spots and dilines on the c(4 × 2) terraces in Fig. 7b. The bright spots are similar to the BaO nanoparticles observed following Ba deposition on the reconstructed SrTiO₃ surface. This indicates that at the initial growth stage of the co-deposition, Ba forms BaO nanoparticles on the surface and Ti again contributes to the familiar c(4 × 2) and (6 × 2) reconstructions.

4. Discussion

With small Ti coverages (below 1.00 ML), the deposited Ti forms a series of SrTiO₃(001) surface reconstructions including c(4 × 2), $\left(\sqrt{5} \times \sqrt{5}\right) - R26.6°$, (6 × 2) and (9 × 2). These structures have previously been obtained by sputtering and/or annealing at relatively high temperatures (above 800 °C) [30,36,40]. In this study, we demonstrate that they can be achieved by careful control of the Ti deposition amount followed by annealing at lower temperatures (below

600 °C). It has been reported that on SrTiO₃(110) and SrTiO₃(111) surfaces, the thermodynamically stable structures vary as a function of Ti concentration [45,46]. An increasing Ti concentration results in the sequential formation of (5 × 1), (4 × 1), (2 × 8) and (6 × 8) reconstructions on SrTiO₃(110) [45,47,48] and the formation of (4 × 4), (6 × 6) and (5 × 5) structures on SrTiO₃(111) [46]. Similarly, on the SrTiO₃(001) surface, the reconstruction evolves from c(4 × 4) to c(4 × 2) and then to $\left(\sqrt{5} \times \sqrt{5}\right) - R26.6°$ with raised Ti coverage. The results provide direct evidence that all the observed SrTiO₃(001) reconstructions including c(4 × 2), $\left(\sqrt{5} \times \sqrt{5}\right) - R26.6°$, (6 × 2) and (9 × 2) are Ti-rich. A $Sr_x TiO_{2+y}$ (x, y < 1) intermediate phase has recently been reported to grow during the pulsed laser deposition of TiO₂ on SrTiO₃(001) as a result of Sr diffusion [39]. Such diffusion is very unlikely to occur in our study due to the relatively low growth temperatures. Also, first principles simulations indicate a double-layer TiO₂ structure for the c(4 × 2) phase [31,32] and triple-layer TiO$_x$ structures for the (6 × 2) and (9 × 2) reconstructions [32,41]. Such studies are consistent with the evolutionary sequence we observed by increasing the Ti coverage on SrTiO₃(001) surfaces and none of the surface structures contains Sr.

If the amount of Ti that forms the SrTiO₃(001) reconstruction is surpassed, the excessive Ti starts to form anatase TiO₂ islands on the SrTiO₃(001) surface as previously reported [19,20]. Anatase islands have also been obtained by extensive UHV annealing (875 °C, 20 h) of a sputtered SrTiO₃(001) sample [43,49], for which sputtering allows Ti enrichment in the near-surface region, and extensive annealing
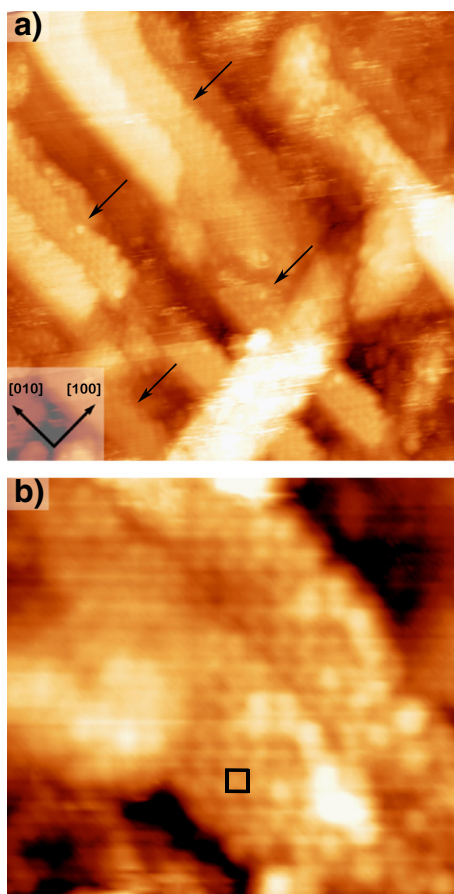
Fig. 6. STM images showing (a) a locally ordered structure indicated by arrows following Ba deposition onto a sputtered $SrTiO_3$ substrate surface with post-annealing (Image size: 46×46 nm^2, $V_s = 1.00$ V, $I_t = 0.20$ nA); (b) details of the ordered structure with a unit cell indicated by the square, enlarged from an image taken from another area on the surface (Image size: 14×13 nm^2, $V_s = 1.28$ V, $I_t = 0.20$ nA).

Fig. 7. STM images showing (a) a disordered surface following Ba and Ti deposition on a degassed $SrTiO_3$ substrate (Image size: 100×100 nm^2, $V_s = 1.07$ V, $I_t = 0.10$ nA); (b) dilines and bright BaO nanoparticles on the $c(4 \times 2)$-reconstructed $SrTiO_3(001)$ surface after UHV annealing of the surface at 800 °C for 1.5 h (Image size: 50×50 nm^2, $V_s = 0.78$ V, $I_t = 0.20$ nA).

facilitates Ti segregation to the surface to form anatase islands [43,49]. In this study, Ti deposition serves as an alternative way to make the surface Ti-rich. The excessive Ti stays on the substrate surface and does not need to diffuse there from the bulk. Therefore, much less thermal energy is required for the formation of epitaxial anatase TiO_2.

For BaO thin film growth on $SrTiO_3$, the small lattice mismatch between BaO and $SrTiO_3$ allows the latter to serve as a suitable substrate for the growth of BaO thin films. The growth mode (islanding or layer-by-layer), however, is partially determined by the substrate surface energy. The reconstructed $SrTiO_3(001)$ substrate exhibits relatively low surface energy, leading to the formation of BaO nanoparticles. Contrastingly, a sputtered substrate with a rough surface which might provide more nucleation sites and a higher surface energy is favorable for the growth of a locally ordered $c(4 \times 4)$ epitaxial BaO structure.

Through Ba and Ti co-deposition, we also explored the possibility of the elemental growth of $BaTiO_3$ thin films on $SrTiO_3(001)$ at the initial growth stages. Instead of forming $BaTiO_3$, the deposited Ti forms the $c(4 \times 2)$ and the (6×2) $SrTiO_3(001)$ reconstructions, while Ba again forms BaO nanoparticles. Considering the large enthalpy of reaction for TiO_2 and BaO to form $BaTiO_3$ (-153 KJ/mol) [50], $BaTiO_3$ films are expected to grow. However, at the very early growth stage, the influence of the surface and interfacial energies dominate. Low surface energies associated with the reconstructed $SrTiO_3(001)$ surfaces lead to phase separation with the formation of BaO nanoparticles and Ti-rich $SrTiO_3(001)$ reconstructions containing multiple TiO_x layers. $BaTiO_3$ is

likely to grow for thicker films as the enthalpy of reaction would then dominate the thermodynamics.

5. Conclusion

In the growth of TiO_2 thin films, increasing amounts of Ti have been deposited onto the $SrTiO_3(001)$ surface and oxidized by residual gases in the chamber and/or O from the substrate. At the early growth stages, the deposited Ti results in the formation of a series of Ti-rich structures including $c(4 \times 2)$, $(\sqrt{5} \times \sqrt{5}) - R26.6°$, (6×2) and (9×2). Since Ti deposition serves as a more efficient way to vary the surface stoichiometry than the previous reported method involving sputtering and/or annealing, these reconstructions can be achieved with much lower temperatures. Epitaxial anatase thin films form with increased Ti coverages (>0.50 ML) and/or post-annealing at relatively high temperatures (>600 °C). Based on the STM and the LEED data, (3×1) and (5×1) reconstructions are obtained on the epitaxial anatase TiO_2 islands grown on $SrTiO_3(001)$.

Different $SrTiO_3(001)$ substrate surfaces are used to obtain epitaxial BaO thin films. Compared with reconstructed substrate surfaces, a disordered $SrTiO_3$ surface allows the formation of a locally ordered $c(4 \times 4)$ BaO structure due to its relatively high surface energy. Despite a high enthalpy of formation of $BaTiO_3$, it is difficult to grow $BaTiO_3$ films on $SrTiO_3$ elementally at the initial growth stages where the influence of the surface and interfacial energy dominates. In order to minimize the overall energy, the deposited Ti forms Ti-

rich surface reconstructions, with the Ba forming BaO nanoparticles on the surface.

Acknowledgment

Appendix A. Supplementary data

Supplementary data to this article can be found online at http://dx.doi.org/10.1016/j.susc.2013.08.019.

References

[1] U. Diebold, Surf. Sci. Rep. 48 (2003) 53.
[2] D.I. Enache, J.K. Edwards, P. Landon, B. Solsona-Espriu, A.F. Carley, A.A. Herzing, M. Watanabe, C.J. Kiely, D.W. Knight, G.J. Hutchings, Science 311 (2006) 362.
[3] B. Seger, T. Pedersen, A.B. Laursen, P.C.K. Vesborg, O. Hansen, I. Chorkendorff, J. Am. Chem. Soc. 135 (2013) 1057.
[4] M.G. Manera, A. Colombelli, R. Rella, A. Caricato, P.D. Cozzoli, M. Martino, L. Vasanelli, J. Appl. Phys. 112 (2012) 053524.
[5] J. Roales, J.M. Pedrosa, P. Castillero, M. Cano, T.H. Richardson, A. Barranco, A.R. Gonzalez-Elipe, ACS Appl. Mater. Interfaces 4 (2012) 5147.
[6] A.A. Haidry, J. Puskelova, T. Plecenik, P. Durina, J. Gregus, M. Truchly, T. Roch, M. Zahoran, M. Vargova, P. Kus, A. Plecenik, G. Plesch, Appl. Surf. Sci. 259 (2012) 270.
[7] M.C. Kao, H.Z. Chen, S.L. Young, C.Y. Kung, C.C. Lin, Thin Solid Films 517 (2009) 5096.
[8] Y.H. Jang, X.K. Xin, M. Byun, Y.J. Jang, Z.Q. Lin, D.H. Kim, Nano Lett. 12 (2012) 479.
[9] P. Swarnakar, S.R. Kanel, D. Nepal, Y.T. Jiang, H.Y. Jia, L. Kerr, M.N. Goltz, J. Levy, J. Rakovan, Sol. Energy 88 (2013) 242.
[10] A. Shih, J.E. Yater, C. Hor, Appl. Surf. Sci. 242 (2005) 35.
[11] A.A. Hashim, A.K. Ray, A.K. Hassan, D.S. Barratt, Appl. Surf. Sci. 243 (2005) 421.
[12] J. Wang, X.M. Wu, L.J. Zhuge, Vacuum 81 (2007) 890.
[13] R.E. Thomas, J.W. Gibson, G.A. Haas, R.H. Abrams Jr., IEEE Trans. Electron Devices 37 (1990) 850.
[14] H. Yang, L. Ma, X.B. Xie, H.F. Yu, Phys. Lett. A 348 (2006) 272.
[15] S. Tuscharoen, J. Kaewkhao, P. Limkitjaroenporn, P. Limsuwan, W. Chewpraditkul, Ann. Nucl. Energy 49 (2012) 109.
[16] G. Paramesh, K.B.R. Varma, J. Am. Ceram. Soc. 95 (2012) 2876.
[17] C.C. Hsieh, K.H. Wu, J.Y. Juang, T.M. Uen, J.-Y. Lin, Y.S. Gou, J. Appl. Phys. 92 (2002) 2518.
[18] L. Miao, S. Tanemura, K. Kaneko, A. Terai, N. Nabatova-Gabain, J. Cryst. Growth 254 (2003) 100.
[19] A. Lotnyk, S. Senz, D. Hesse, Thin Solid Films 515 (2007) 3439.
[20] Y. Du, D.J. Kim, T.C. Kaspar, S.E. Chamberlin, I. Lubinetsky, S.A. Chambers, Surf. Sci. 606 (2012) 1443.
[21] R. Kita, T. Hase, T. Takahashi, K. Kawaguchi, T. Morishita, J. Mater. Res. 8 (1993) 321.
[22] T. Ohnishi, M. Yoshimoto, G.H. Lee, T. Maeda, H. Koinuma, J. Vac. Sci. Technol. A 15 (1997) 2469.
[23] M. Kubo, Y. Oumi, R. Miura, A. Stirling, A. Miyamoto, M. Kawasaki, M. Yoshimoto, H. Koinuma, J. Chem. Phys. 109 (1998) 9148.
[24] S.B. Mi, C.L. Jia, T. Heeg, O. Trithaveesak, J. Schubert, K. Urban, J. Cryst. Growth 283 (2005) 425.
[25] Y.R. Li, J.L. Li, Z. Jun, Z. Ying, H.Z. Zeng, X.H. Wei, J.L. Tang, Appl. Phys. Lett. 88 (2006) 152901.
[26] D.A. Tenne, P. Turner, J.D. Schmidt, M. Biegalski, Y.L. Li, L.Q. Chen, A. Soukiassian, S. Trolier-McKinstry, D.G. Schlom, X.X. Xi, D.D. Fong, P.H. Fuoss, J.A. Eastman, G.B. Stephenson, C. Thompson, S.K. Streiffer, Phys. Rev. Lett. 103 (2009) 177601.
[27] S.H. Phark, Y.J. Chang, T.W. Noh, Appl. Phys. Lett. 98 (2011) 161908.
[28] F. Silly, D.T. Newell, M.R. Castell, Surf. Sci. Lett. 600 (2006) L219.
[29] M.R. Castell, Surf. Sci. 505 (2002) 1.
[30] M.R. Castell, Surf. Sci. 516 (2002) 33.
[31] N. Erdman, O. Warschkow, M. Asta, K.R. Poeppelmeier, D.E. Ellis, L.D. Marks, J. Am. Chem. Soc. 125 (2003) 10050.
[32] A.E. Becerra-Toledo, M.S.J. Marshall, M.R. Castell, L.D. Marks, J. Chem. Phys. 136 (2012) 214701.
[33] H. Tanaka, T. Matsumoto, T. Kawai, S. Kawai, Surf. Sci. 318 (1994) 29.
[34] Z. Fang, K. Terakurac, Surf. Sci. 470 (2000) L75.
[35] T. Kubo, H. Nozoye, Phys. Rev. Lett. 86 (2001) 1801.
[36] T. Kubo, H. Nozoye, Surf. Sci. 542 (2003) 177.
[37] D.T. Newell, A. Harrison, F. Silly, M.R. Castell, Phys. Rev. B 75 (2007) 205429.
[38] I. Shirakia, K. Miki, Surf. Sci. 605 (2011) 1304.
[39] M. Radovic, M. Salluzzo, Z. Ristic, R. Di Capua, N. Lampis, R. Vaglio, F.M. Granozio, J. Chem. Phys. 135 (2011) 034705.
[40] D.S. Deak, F. Silly, D. Newell, M.R. Castell, J. Phys. Chem. B 110 (2006) 9246.
[41] M.S.J. Marshall, A.E. Becerra-Toledo, D.J. Payne, R.G. Egdell, L.D. Marks, M.R. Castell, Phys. Rev. B 86 (2012) 125416.
[42] M.S.J. Marshall, A.E. Becerra-Toledo, L.D. Marks, M.R. Castell, Phys. Rev. Lett. 107 (2011) 086102.
[43] F. Silly, M.R. Castell, Appl. Phys. Lett. 85 (2004) 3223.
[44] Y. Liang, S. Gan, S.A. Chambers, Phys. Rev. B 63 (2001) 235402.
[45] Z. Wang, F. Yang, Z. Zhang, Y. Tang, J. Feng, K. Wu, Q. Guo, J. Guo, Phys. Rev. B 83 (2011) 155453.
[46] J. Feng, X. Zhu, J. Guo, Surf. Sci. 614 (2013) 28.
[47] J.A. Enterkin, A.K. Subramanian, B.C. Russell, M.R. Castell, K.R. Poeppelmeier, L.D. Marks, Nat. Mater. 9 (2010) 245.
[48] F. Li, Z. Wang, S. Meng, Y. Sun, J. Yang, Q. Guo, J. Guo, Phys. Rev. Lett. 107 (2011) 036103.
[49] M.S.J. Marshall, M.R. Castell, Phys. Rev. Lett. 102 (2009) 146102.
[50] E. Takayama-Muromachi, A. Navrotsky, J. Solid State Chem. 72 (1988) 244.